Characterization of the CYP3A4 Active Site by Homology Modeling

Toshimasa TANAKA,* Teruaki OKUDA, and Yoshio YAMAMOTO

Pharmaceutical Research Division, Takeda Chemical Industries, Ltd.; 2–17–85 Juso-Honmachi, Yodogawa-ku, Osaka 532–8686, Japan. Received March 8, 2004; accepted April 14, 2004; published online April 19, 2004

Human microsomal cytochrome P450s participate in drug metabolism and detoxification. Among them, CYP3A4 is the most important isoform for drug–drug interactions. To gain a better understanding of the active site, a homology model of CYP3A4 was constructed based on the crystallographic coordinates of mammalian CYP2C5. The putative active site is much larger than that of CYP2C5 and is divided into three parts (*i.e.* a proximal and two distal sites from the heme). Most residues reported to be important for ligand-binding are located in the active site of the model. Moreover, some inhibitors (paclitaxel *etc.*) docked into the model have complementary shapes to the pocket. Pharmacophore docking of 14 substrates was also performed using Ph4Dock of MOE. Calculated interaction energies showed a moderate correlation with the logarithm of apparent K_m values. These results suggest that this model is reliable enough to be used in the design of compounds for removing undesirable CYP3A4 inhibition.

Key words CYP3A4; homology modeling; docking model; Ph4Dock; drug–drug interaction; cytochrome P450

Cytochrome P450s (CYPs) are membrane-associated heme proteins and hepatic microsomal enzymes, which participate in drug metabolism and detoxification. Among more than 50 human CYPs, an isoform, CYP3A4, is a major enzyme responsible for drug–drug interactions that is concerned in at least 50% of drug metabolism.[1] In addition, CYP3A4 is expressed at a high level in the human liver.[2] Thus, it is important to know the CYP3A4 inhibitory potency of new drug candidates at an early stage of drug discovery. Although many detailed studies about CYP3A4 inhibitory pharmacophores have been published,[3] precise interactions between inhibitors (or substrates) and CYP3A4 have not been defined well. Recently, the crystal structure of CYP2C5 was determined by Williams *et al.*,[4] which is the first structure of a mammalian microsomal CYP. To understand the molecular basis of CYP3A4 inhibition well, a CYP3A4 homology model was constructed, and inhibitors and substrates were docked into the model. In this report we will describe some interesting features of the putative active site of CYP3A4.

Experimental

Homology Modeling The amino acid sequence of CYP3A4 was taken from the ExPASy web site (http://tw.expasy.org/). The amino acid sequence alignment used for the homology modeling was obtained as follows. The amino acid sequences for which 3D structures were available at the time (*Pseudomonas-Putida* $P450_{CAM}$,[5] *Pseudomonas-SP* $P450_{TERP}$,[6] *Saccharopolyspora-Erythraea* $P450_{eryF}$,[7] *Fusarium-Oxysporum* $P450_{NOR}$,[8] *Bacillus-Megaterium* $P450_{BM3}$,[9,10] and mammalian CYP2C5[4]) were aligned according to their 3D structures using the homology module of Insight II (ver. 2000, Accelrys Inc., San Diego, California, U.S.A.). Subsequently, amino acid sequences of human metabolic CYPs were aligned by sequence homology using ClustalW.[11] The combined alignments were manually revised so that insertions and deletions did not get into the portions corresponding to probable secondary structures, as far as possible, and the following four characteristic motifs of CYPs were aligned: WXXXR (where W is tryptophan, R is arginine, and X is any amino acid) in the alpha-helix C, EXXR (where E is glutamate, R is arginine, and X is any amino acid) in the alpha-helix K, ZXXPXXZXPXXZ (where P is proline, Z is aromatic amino acid, and X is any amino acid) after the alpha-helix K′ and FXXGXXXCXG (where F is phenylalanine, G is glycine, C is cysteine, and X is any amino acid) before the alpha-helix L.[12]

According to the alignment (Fig. 1), a homology model of CYP3A4 was constructed based on the crystal structure of mammalian CYP2C5 (PDB code:1DT6) using the homology module of Insight II. Although the sequence identities between CYP102 (BM3) and CYP3A4 versus CYP2C5 and CYP3A4 are very similar (22%), CYP2C5 was chosen as a template since the mammalian CYP was presumed to be more suitable than a prokaryotic one. Using the Search/Generate-Loops function of Insight II, conformations of the insertion and deletion parts in the alignment were obtained referring to the known 3-D structures. After some manual adjustments to remove large steric hindrances, the whole structure was subjected to energy minimization for 1000 steps with the steepest descent minimizer, and subsequently 5000 steps with the conjugate gradient minimizer, to a maximum gradient of 0.1 kcal/mol^{-1} Å^{-1}, using the Discover-ESFF force field (ver 980, Accelrys Inc., San Diego, California, U.S.A.). During the minimization procedure, the following conditions were adopted. The dielectric constant was set to 4*r, where r is the distance between two interacting atoms. The force constant of tethering constraints for the backbone of structurally conserved regions (SCRs, asterisks in Fig. 1) and heme was set to 40 kcal/Å^2 to prevent a large movement from the initial positions.

Docking of Inhibitors Covalent bonding models of imidazole and methylendioxyphenyl were constructed by full energy minimization using the Discover-ESFF force field. Then, the residual parts of ketoconazole (IC_{50} value for CYP3A4 $<0.1\,\mu M$[13]) and a methylenedioxyphenyl compound (3,4-dihydro-2-[5-methoxy-2-[3-[*N*-[2-[*N*-(*t*-butoxycarbonyl)amino]ethyl]-*N*-[2-(3,4-methylenedioxy)ethyl]amino]propoxy]phenyl]-4-methyl-3-oxo-2*H*-1,4-benzothiazine; IC_{50} value for CYP3A4$=6.9\,\mu M$[14]) were connected to the imidazole and methylendioxyphenyl structures obtained above, respectively. Using the Search–Compare module of Insight II, the stable binding mode of each compound was explored by systematic bond rotation within the ligand, including some side chains around the ligand, and energy minimization was continued using the Discover-ESFF force field. The condition of the energy minimization is the same as that described in the homology modeling section.

Paclitaxel (an anticancer drug) and losartan (an antihypertensive) were docked into the CYP3A4 model using Gold (ver. 2.0, the Cambridge crystallographic data centre, U.K.[15]) with the standard default settings.

Pharmacophore Docking of Substrates Pharmacophore Dock (Ph4Dock,[16]) of MOE (ver. 2003.02, Chemical Computing Group: Montreal, Canada) was performed for losartan and typical CYP3A4 substrates (saquinavir,[17] indinavir,[18] quinidine,[19] nifedipine,[20] terfenadine,[21] ritonavir,[22] dexamethasone,[23] verapamil,[24] erythromycin,[25] testosterone,[25] tamoxifen,[26] fentanyl,[27] amiodarone,[28] and colchicine[29]). A pharmacophore model for CYP3A4 ligands was manually created based on the docking models of ketoconazole and the methylenedioxyphenyl derivative described above (Fig. 5). Exclusive volumes were automatically generated with Ph4Dock according to the atomic positions of the CYP3A4 model. Interaction energy ($U_{ele}+U_{vdw}$; *i.e.*, summation of intermolecular electrostatic and van der Waals energy) was calculated after energy minimization, which was carried out by the MMFF94s force field[30,31] for substrate molecules and the side chains of the enzyme within 4.5 Å of each substrate.

* To whom correspondence should be addressed. e-mail: Tanaka_Toshimasa@takeda.co.jp

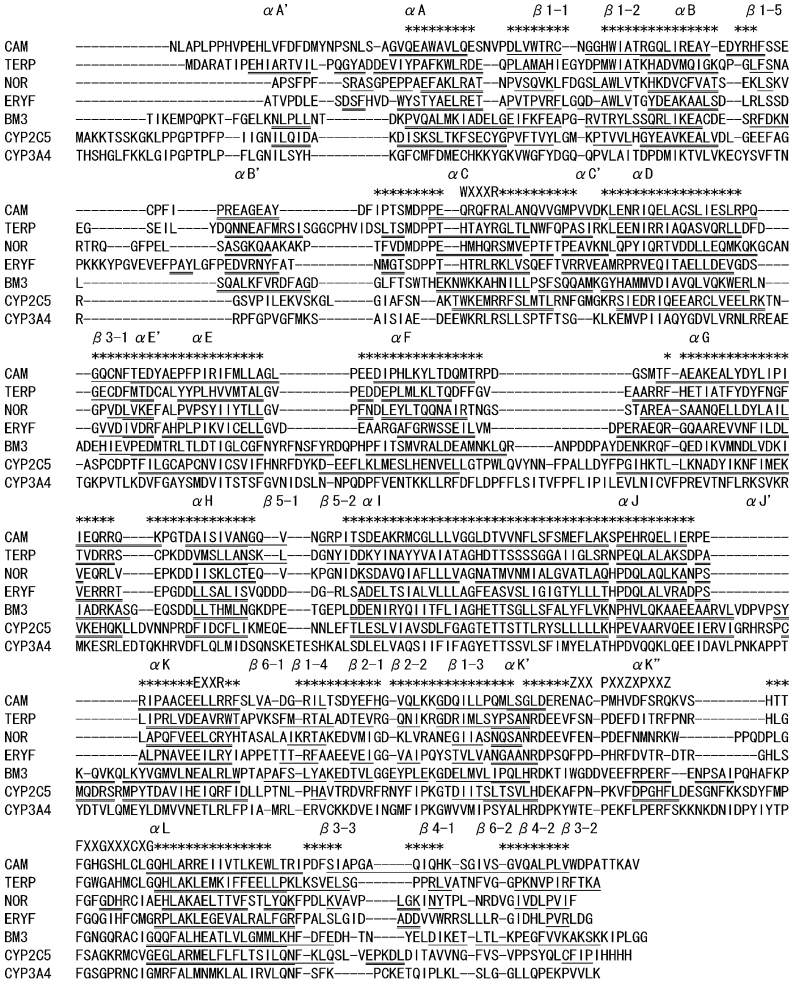

Fig. 1. Alignment of Amino Acid Sequences among $P450_{CAM}$,[5] $P450_{TERP}$,[6] $P450_{eryF}$,[7] $P450_{NOR}$,[8] $P450_{BM3}$,[9,10] CYP2C5,[4] and CYP3A4

Alpha-helices and beta-sheets are shown by double and single underlines, respectively. Asterisks indicate structurally conserved regions (SCRs) among the known 3-D structures.

Results and Discussion

The active-site pocket of the CYP3A4 model is much larger (950 Å^3) than the CYP2C5 crystal structure (420 Å^3). In addition, the pocket is divided into three parts, a proximal site and two distal sites from the heme. The larger pocket of CYP3A4 is attributed to the existence of an additional pocket (the distal pocket 2 in Fig. 2), and is consistent with the broad substrate selectivity of CYP3A4. In the CYP3A4 model, the approach to the additional pocket is comprised of Pro110, Ile120, Asp214, Leu373, and Leu479. On the other hand, the larger amino acids of CYP2C5 (Ile102, Phe114, Leu208, Leu363, and Phe473) occlude access to the additional pocket. The positions of the important residues for substrate-binding[32—39] (Table 1), which were confirmed by site-directed mutagenesis, were also checked in the CYP3A4 model. Except for two of them (Asn206 and Val376), most of the important residues were formed in the binding pocket (Pro107, Phe108, Ser119, Ile120, Leu210, Leu211, Asp214, Ile301, Phe304, Ala305, Thr309, Ile369, Ala370, Leu373, Ser478, and Leu479; Fig. 3a). The Ramachandran plot analyzed by the program Prockeck[40] to check the stereochemical quality, indicates that 99% of non-Gly and non-Pro residues exist in the allowed regions (Fig. 3b). Although the sequence identity between CYP3A4 and CYP2C5 is only 22%, the above result indicates the validity of the model.

Ketoconazole, which was bound in the proximal and the distal site 2, has a length similar to that of the putative binding pocket (*ca.* 18 Å, Fig. 4a). On the other hand, the BOC substituent of the methylenedioxyphenyl derivative was docked in the first distal site (distal site 1), and this molecule used all the three sites for binding (Fig. 4b). The conformations of docked ketoconazole and the methylendioxyphenyl derivative had very similar length in the active-site pocket of the CYP3A4 model. The results are consistent with the facts that shorter and longer analogs of ketoconazole (*e.g.* fluconazole and itraconazole, respectively) are weaker inhibitors of CYP3A4[41] and shorter analogs of the methylenedioxyphenyl derivative show lower activity for CYP3A4.[14] The accordance in terms of the length also confirms the validity of the model. Covalent type inhibitors were chosen for docking to reduce ambiguity over their binding modes. It is generally accepted that sterically unhindered N-containing heterocycles (*e.g.* pyridine, imidazole, and, triazole) make a coordinate bond with the heme iron, as seen in the crystal structure of $P450_{CAM}$ with a bound pyridine derivative[42]. Methylenedioxyphenyl derivatives are also thought to make covalent bonds by attacking the heme iron from a methylene bridge carbene.[14] These N-containing heterocycle and methylene-

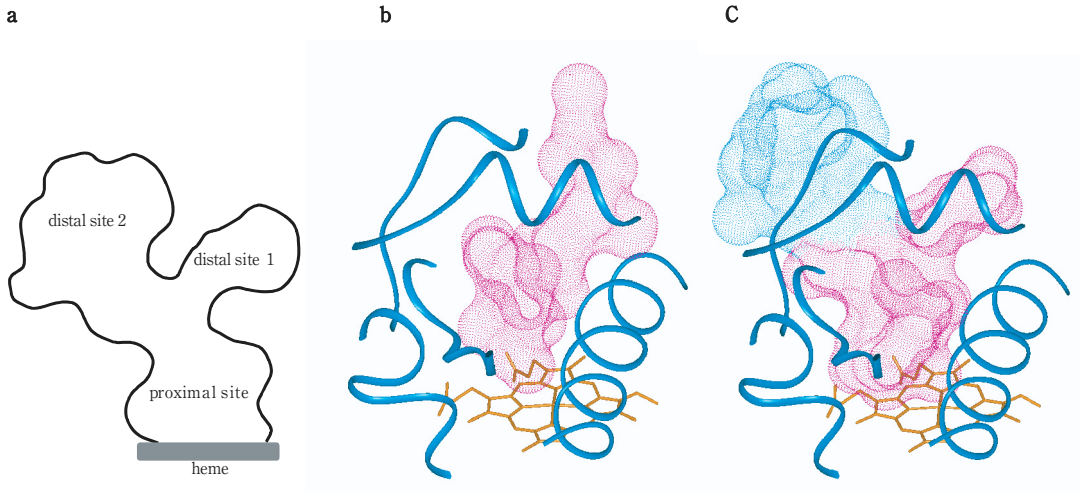

Fig. 2. (a) Diagram Sketch of Three Parts of the Putative Active Site, (b) the Pocket of the CYP2C5 Crystal Structure and (c) the Pocket of the CYP3A4 Model

Magenta dot surface indicates the shape of the proximal site and the distal site 1. Blue dot surface indicates the shape of the distal site 2 (the additional pocket).

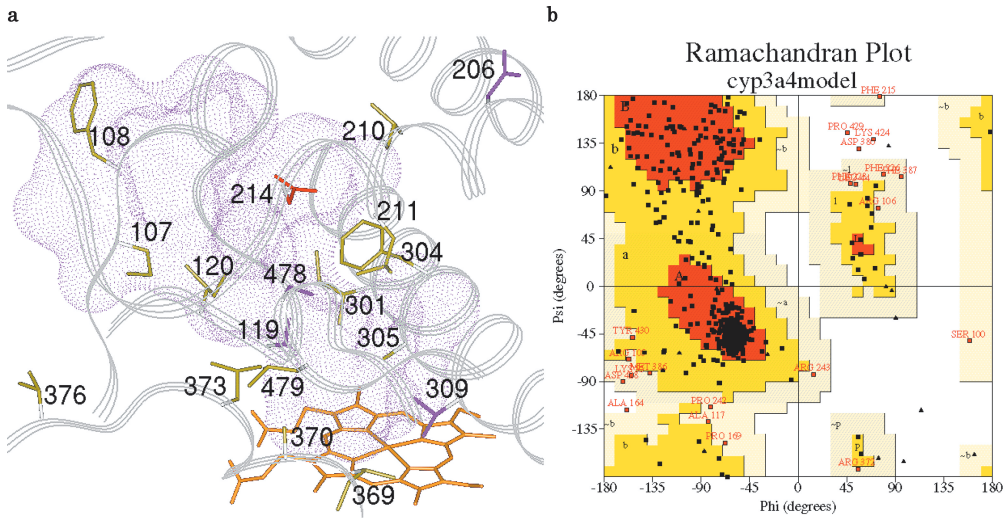

Fig. 3. (a) Distribution of the Amino Acid Residues Reported as Important Sites for Ligand-Binding

Heme is displayed in orange, acidic residues in red, basic residues in blue, polar residues in magenta and hydrophobic residues in yellow. Magenta dot surface indicates the shape of the pocket.

(b) Ramachandran Plot of the CYP3A4 Model Analyzed by Procheck

Table 1. Important Residues for CYP3A4 Substrate Recognition

Substrate	Residue	Reference
Testosterone	S119, I301, A305, L373	32, 33
Progesterone	S119, F304, A305, T309, I369, A370, L373	32, 33, 34
Aflatoxin B1	P107, N206, L210, I369, V376, S478, L479	35
RPR 106541	L210, I301, F304, A305, A370, L479	36
7-Hexoxycoumarin	S119, L210, I301, A305, A370, L373, L479	37
Midazolam	F108, I120, I301, F304, T309	38
Alpha-naphtoflavone	L211, D214	39

dioxyphenyl derivatives are useful for elucidating the general features of the active-site pockets of CYPs.

Paclitaxel is hydroxylated by CYP3A4 at the phenyl ring of the C3′ position.[43] Ten docking modes of paclitaxel offered by Gold were similar to each other. In the docking modes, paclitaxel has an orientation that can account for the metabolite formation (Fig. 5a). The bulky taxane skeleton was docked in the distal site 2, which is the largest of the three sites in the pocket.

On the other hand, various bound orientations of losartan

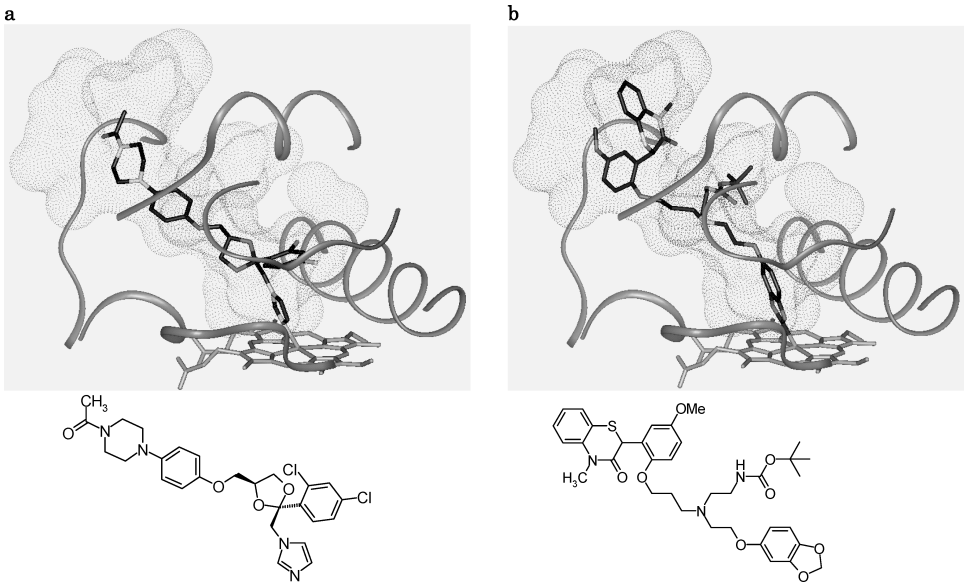

Fig. 4. Docking Models of Bond-Forming Inhibitors, (a) Ketoconazole and (b) a Methylendioxyphenyl Derivative

Dot surface indicates the shape of the pocket and main chain around the pocket is depicted as ribbon.

Table 2. Inhibitory Activity of Angiotensin II Antagonists for CYP3A4 (IC_{50} Value: μM[44])

	Losartan	Irbesartan	Eprosartan	Valsartan	Candesartan
CYP3A4	210	224	>1000	>1000	>600

Table 3. Apparent K_m Values (μM) and Interaction Energy (kcal/mol) Calculated by Ph4Dock

Substrate	K_m	Rank	$U_{vdw}+U_{ele}$	Rank	$U_{vdw}+U_{ele}$	U_{vdw}	U_{ele}	Reference
Saquinavir	0.35	1	−617.3	6	−496.9	284.4	−781.3	17
Indinavir	1.3	1	−407.4	1	−407.4	269.1	−676.5	18
Quinidine	4	1	−390.4	2	−388.9	207.5	−596.4	19
Nifedipine	9	1	−418.6	1	−418.6	259.1	−677.7	20
Terfenadine	9.6	1	−479	5	−390.8	325.7	−716.5	21
Ritonavir	20	1	−442.4	3	−353.1	277.1	−630.2	22
Dexamethasone	23.2	1	−408.8	1	−408.8	244.1	−652.9	23
Verapamil	49	1	−511.9	3	−394.1	359.4	−753.5	24
Erythromycin	61	1	−441.3	4	−362.6	354.4	−717.0	25
Testosterone	90.5	1	−388	1	−388	246.7	−634.7	25
Tamoxifen	98	1	−352.1	1	−352.1	215.7	−567.8	26
Fentanyl	117	1	−336	1	−336	215.2	−551.2	27
Amiodarone	310	1	−427.1	7	−361.8	301.1	−662.9	28
Colchicine	5600	1	−221.2	1	−221.2	157.7	−378.9	29

Rank indicates the ranking in orientation candidates obtained by Ph4Dock. $U_{vdw}+U_{ele}$ is the sum of interaction energy (van der Waals+electrostatic) calculated by MMFF94s force field. The last five columns are for the orientations consistent with the metabolite formation.

(IC_{50} value for CYP3A4 is 210 μM[44]) were generated by Gold. The most reasonable binding mode of losartan, therefore, was explored using the pharmacophore docking program Ph4Dock in MOE. Pharmacophore dock is a new docking methodology, which involves a ligand-based pharmacophore being introduced in an automated docking method. The merit of Ph4Dock is that the binding mode consistent with a predicted ligand-based pharmacophore can be obtained considering structural information of a protein. The pharmacophore used here for Ph4Dock consists of 7 hydrophobic areas, 3 hydrogen bond donor sites, and 2 hydrogen bond donor and acceptor sites (Fig. 6). In the procedure, the flexibility of side chains around the ligand was considered by energy minimization of the complex.

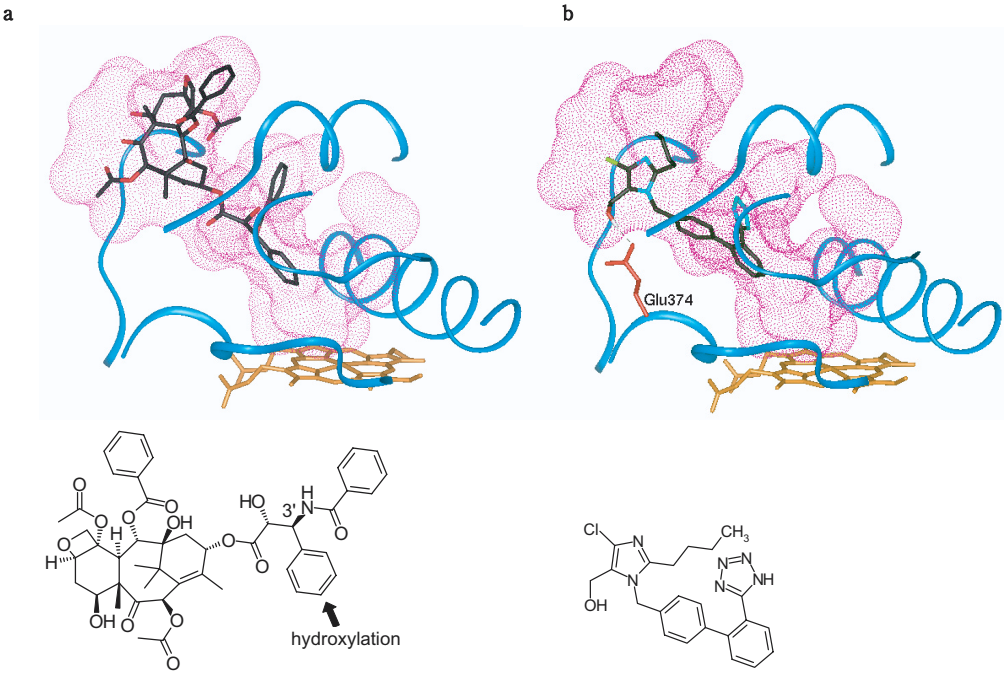

Fig. 5. Docking Models of (a) Paclitaxel and (b) Losartan

Magenta dot surface indicates the shape of the pocket and main chain around the pocket is depicted as cyan ribbon.

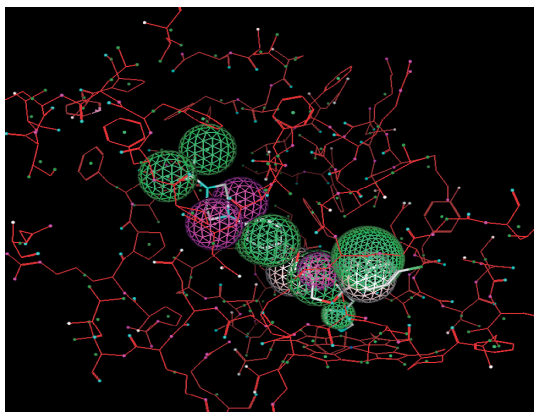

Fig. 6. Pharmacophore Used for Ph4Dock of MOE

The pharmacophore consists of hydrophobic regions (green mesh spheres), hydrogen bond donor sites (magenta mesh spheres), and hydrogen bond donor and acceptor sites (beige mesh spheres). Red wires indicate the CYP3A4 model. Exclusive volumes are omitted for clarity. Ketoconazole docked in the model is superimposed (white stick).

Ph4Dock predicted a single binding mode, in which the hydroxy group of losartan forms a hydrogen bond with the side chain of Glu374, which is located at the approach to the distal site 2 (Fig. 5b). It is reported that losartan and irbesartan exhibit week affinity toward CYP3A4, whereas eprosartan, valsartan, and candesartan have no affinity (Table 2[44]). The difference of affinity for CYP3A4 may be derived from the existence of a carboxylic acid at the equivalent position to the hydroxy group of losartan. It may be assumed that the minus charge of the carboxylic acid will repel the side chain of the glutamate. In addition to Glu374, two acidic amino acids (Asp214 and Asp217) exist at the approach to the distal site 2. If our analysis about the sartans is correct, introduction of an acidic substituent at an appropriate position could be a good way of solving the CYP3A4 inhibitory problem.

To examine whether bound orientations and binding potency of substrates can be predicted with a reasonable accuracy, pharmacophore docking for typical CYP3A4 substrates was carried out using Ph4Dock, using the procedure described above. As shown in Table 3, half the top-rank models were consistent with the formation of their metabolites. Interaction energies for the 14 substrates were then plotted against the logarithm of the published apparent K_m values (Table 3). When the top-rank model was adopted for each compound, the correlation was not so good (Fig. 7a; the R^2 value is 0.532). On the other hand, by selecting the orientation consistent with each metabolite formation, a moderate correlation was obtained (Fig. 7b; the R^2 value is 0.779). It was also found that the electrostatic interaction energy contributes more than the van der Waals energy, especially when saquinavir and colchicine are compared (Table 3). The precise cause could not be determined, but the interaction with the acidic amino acids (*e.g.* Glu374, Asp214 and Asp217) might be one of the reasons. Although other factors have to be considered to improve the correlation, a combination of Ph4Dock and molecular orbital calculations, which can be used for predicting metabolizable positions, should be extremely useful.

Conclusions

We have constructed a homology model of CYP3A4, the most important isoform of human CYPs for drug–drug interactions. The structure is based on the crystallographic coordinates of mammalian CYP2C5. The relatively large active-site pocket of the model, which is consistent with the broad substrate selectivity of CYP3A4, is divided into three parts (a proximal and two distal sites from the heme). Most of the

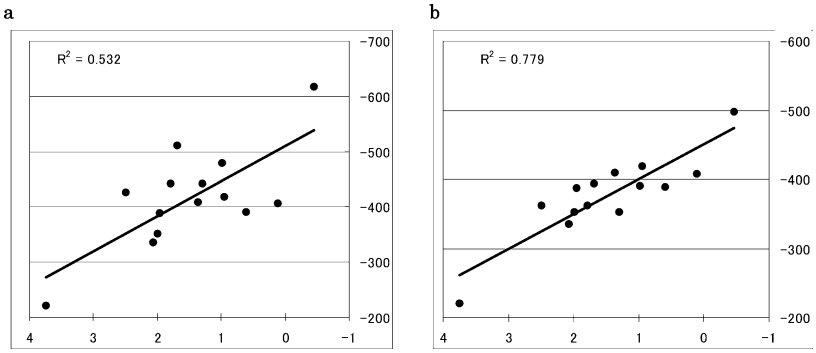

Fig. 7. Correlation Plots between the Logarithm of Apparent K_m Values (Horizontal Axis) and Interaction Energy (Vertical Axis)
(a) The case where only top-rank binding modes are used, and (b) the case where the binding modes consistent with the metabolite formation are used.

residues that have been reported to be important for ligand-binding are located in the active site.

Ketoconazole and the methylenedioxyphenyl derivative docked into the model have a length similar to that of the putative pocket. Paclitaxel bound to the model is also complementary to the shape of the pocket and has an orientation that is consistent with the observed metabolite formation. In the binding model of losartan, the hydroxy group is assumed to form a hydrogen bond with the side chain of Glu374, which might be the reason for the lack of affinity of some sartans with carboxylic acid moieties at the equivalent position to the hydroxy group of losartan.

The interaction energies calculated with Ph4Dock show a moderate correlation with the reported K_m values. From this result, it is expected that this CYP3A4 model is reliable enough to be used in the design of compounds for removing undesirable CYP3A4 inhibition.

References and Notes

1) Bertz R. J., Granneman G. R., *Clin. Pharmacokinet.*, **32**, 210—258 (1997).
2) Shimada T., Yamazaki H., Mimura M., Inui Y., Guengerich F. P., *J. Pharmacol. Exp. Ther.*, **270**, 414—423 (1994).
3) de Groot M. J., Ekins S., *Adv. Drug Deliv. Rev.*, **54**, 367—383 (2002).
4) Williams P. A., Cosme J., Sridhar V., Johnson E. F., McRee D. E., *Mol. Cell*, **5**, 121—131 (2000).
5) Poulos T. L., Finzel B. C., Howard A. J., *Biochemistry*, **25**, 5314—5322 (1986).
6) Hasemann C. A., Ravichandran K. G., Peterson J. A., Deisenhofer J., *J. Mol. Biol.*, **236**, 1169—1185 (1994).
7) Cupp-Vickery J. R., Poulos T. L., *Nat. Struct. Biol.*, **2**, 144—153 (1995).
8) Shimizu H., Obayashi E., Gomi Y., Arakawa H., Park S. Y., Nakamura H., Adachi S., Shoun H., Shiro Y., *J. Biol. Chem.*, **275**, 4816—4826 (2000).
9) Ravichandran K. G., Boddupalli S. S., Hasermann C. A., Peterson J. A., Deisenhofer J., *Science*, **261**, 731—736 (1993).
10) Li H., Poulos T. L., *Acta Crystallogr. D*, **51**, 21—32 (1995).
11) Thompson J. D., Higgins D. G., Gibson T. J., *Nucleic Acids Res.*, **22**, 4673—4680 (1994).
12) Lewis D. F., Watson E., Lake B. G., *Mutat. Res.*, **410**, 245—270 (1998).
13) Strolin Benedetti M., Bani M., *Drug Metab. Rev.*, **31**, 665—717 (1999).
14) Nakajima M., Suzuki M., Yamaji R., Takashina H., Shimada N., Yamazaki H., Yokoi T., *Xenobiotica*, **29**, 1191—1202 (1999).
15) Jones G., Willett P., Glen R. C., Leach A. R., Taylor R., *J. Mol. Biol.*, **267**, 727—748 (1997).
16) Goto J., Kataoka R., Hirayama N., *J. Am. Chem. Soc.*, to be submitted.
17) Fitzsimmons M. E., Collins J. M., *Drug Metab. Dispos.*, **25**, 256—266 (1997).
18) Lin J. H., Chiba M., Balani S. K., Chen I. W., Kwei G. Y., Vastag K. J., Nishime J., *Drug Metab. Dispos.*, **24**, 1111—1120 (1996).
19) Guengerich F. P., Muller-Enoch D., Blair I. A., *Mol. Pharmacol.*, **30**, 287—295 (1986).
20) Guengerich F. P., Martin M. V., Beaune P. H., Kremers P., Wolff T., Waxman D. J., *J. Biol. Chem.*, **261**, 5051—5060 (1986).
21) Rodrigues A. D., Mulford D. J., Lee R. D., Surber B. W., Kukulka M. J., Ferrero J. L., Thomas S. B., Shet M. S., Estabrook R. W., *Drug Metab. Dispos.*, **23**, 765—775 (1995).
22) Kumar G. N., Rodrigues A. D., Buko A. M., *J. Pharmacol. Exp. Toxicol.*, **277**, 423—431 (1996).
23) Gentile D. M., Tomlinson E. S., Maggs J. L., Park B. K., Back D. J., *J. Pharmacol. Exp. Ther.*, **277**, 105—112 (1996).
24) Kroemer H. K., Echizen H., Heidemann H., Eichelbaum M., *J. Pharmacol. Exp. Ther.*, **260**, 1052—1057 (1992).
25) Wang R. W., Newton D. J., Scheri T. D., Lu A. Y., *Drug Metab. Dispos.*, **25**, 502—507 (1997).
26) Jacolot F., Simon I., Dreano Y., Beaune P., Riche C., Berthou F., *Biochem. Pharmacol.*, **41**, 1911—1919 (1991).
27) Feierman D. E., Lasker J. M., *Drug Metab. Dispos.*, **24**, 932—939 (1996).
28) Fabre G., Julian B., Saint-Aubert B., Joyeux H., Berger Y., *Drug Metab. Dispos.*, **21**, 978—985 (1993).
29) Tateishi T., Soucek P., Caraco Y., Guengerich F. P., Wood A. J., *Biochem. Pharmacol.*, **53**, 111—116 (1997).
30) Halgren T. A., *J. Comput. Chem.*, **20**, 720—729 (1999).
31) Halgren T. A., *J. Comput. Chem.*, **20**, 730—748 (1999).
32) He Y. A., He Y. Q., Szklarz G. D., Halpert J. R., *Biochemistry*, **36**, 8831—8839 (1997).
33) Domanski T. L., Liu J., Harlow G. R., Halpert J. R., *Arch. Biochem. Biophys.*, **350**, 223—232 (1998).
34) Harlow G. R., Halpert J. R., *J. Biol. Chem.*, **272**, 5396—5402 (1997).
35) Wang H., Dick R., Yin H., Licad-Coles E., Kroetz D. L., Szklarz G., Harlow G., Halpert J. R., Correia M. A., *Biochemistry*, **37**, 12536—12545 (1998).
36) Stevens J. C., Domanski T. L., Harlow G. R., White R. B., Orton E., Halpert J. R., *J. Pharmacol. Exp. Ther.*, **290**, 594—602 (1999).
37) Khan K. K., Halpert J. R., *Arch. Biochem. Biophys.*, **373**, 335—345 (2000).
38) Khan K. K., He Y. Q., Domanski T. L., Halpert J. R., *Mol. Pharmacol.*, **61**, 495—506 (2002).
39) Harlow G. R., Halpert J. R., *Proc. Natl. Acad. Sci. U.S.A.*, **95**, 6636—6641 (1998).
40) Laskowski R. A., MacArthur M. W., Moss D. S., Thornton J. M., *J. Appl. Cryst.*, **26**, 283—291 (1993).
41) Benedetti M. S., Bani M., *Drug Metab. Rev.*, **31**, 665—717 (1999).
42) Raag R., Li H., Jones B. C., Poulos T. L., *Biochemistry*, **32**, 4571—4578 (1993).
43) Monsarrat B., Chatelut E., Royer I., Alvinerie P., Dubois J., Dezeuse A., Roché H., Cros S., Wright M., Canal P., *Drug Metab. Dispos.*, **26**, 229—233 (1998).
44) Taavitsainen P., Kiukaanniemi K., Pelkonen O., *Eur. J. Clin. Pharmacol.*, **56**, 135—140 (2000).